± 0.001 K. A negative nn interaction together with a small and positive nnn one is characteristic of type I fcc antiferromagnetic systems.[27,39] The magnetic structure then may consist of ferromagnetic (001) planes that are antiferromagnetically aligned with the neighboring (001) planes as represented in Figure 4. Accordingly, the magnetic moment of every ion aligns antiparallel with respect to eight first neighbors and parallel with respect to the remaining four. In addition, there are six second neighbors with their magnetic moments aligned also parallel to the central one. In other words, every ion is antiferromagnetically coupled, with two-thirds of its nn being ferromagnetically coupled with the rest of its nn plus with all its nnn.

(39) Tahir-Kheli, R. A.; Callen, H. B.; Jarrett, H. *J. Phys. Chem. Solids* **1966**, *27*, 23.

Neutron diffraction experiments and theoretical work are in progress in order to obtain an experimental determination of the magnetic structure and a better understanding of the magnetic behavior of this compound.

Acknowledgment. The research in Zaragoza and Barcelona has been supported by Grant No. MAT88-0174, from the Comision Interministerial de Ciencia y Tecnología. The research in Chicago has been supported by Grants No. DMR-8515224 and DMR-8815798 from the Solid State Chemistry Program, Division of Materials Research of the National Science Foundation. Cooperative work has been supported by Grant CCB-8504/001 from the American-Spain Joint Committee for Technical and Scientific Cooperation. M.C.M. also acknowledges a student fellowship from the Ministerio de Educación y Ciencia.

Registry No. $[Co(NH_3)_6][FeCl_6]$, 15928-89-9.

Contribution from the Physical Chemistry and Analytical Chemistry Departments, General Motors Research Laboratories, Warren, Michigan 48090-9055

Electrochemistry and Electrochromism of Vanadium Hexacyanoferrate

Michael K. Carpenter,* Robert S. Conell, and Steven J. Simko

Received May 2, 1989

Vanadium hexacyanoferrate (VHCF) is an electrochromic material closely related structurally to Prussian blue. The deposition, characterization, and spectroelectrochemistry of films of VHCF are reported here. The electrodeposition of VHCF films is shown to involve the reduction of vanadium(V) ion in the presence of ferricyanide ion. X-ray diffraction data confirm a cubic crystal structure for VHCF, similar to that of Prussian blue. However, chemical analyses give a higher than expected ratio of V to Fe, which suggests the presence of interstitial vanadium. While VHCF films are visually electrochromic, switching from green in the oxidized state to yellow in the reduced state, UV-vis-near-IR spectra show that most of the electrochromic modulation occurs in the ultraviolet region. From X-ray photoelectron spectroscopy and coulometric results, coupled with other electrochemical data, we conclude that the electrochromic reaction involves only the oxidation and reduction of the iron centers in the compound. The vanadium ions, found to be present predominantly in the +4 state, are unaffected by the reaction. Multiple ferrous sites are suggested to be responsible for the complex electrochemistry of VHCF.

Introduction

Electrochromic materials have received much attention recently because of their possible application in so-called "smart windows"—windows that exhibit dynamically variable light transmission characteristics.[1-3] One of the most durable electrochromic materials reported to date is Prussian blue, a mixed-valence compound with the nominal formula of $KFe[Fe(CN)_6]$.[4-6] Films of Prussian blue that have been deposited on conductive substrates can be electrochemically reduced in the presence of potassium or other alkali-metal ions, according to reaction 1, to

$$\underset{\text{Prussian blue}}{KFe^{III}Fe^{II}(CN)_6} + K^+ + e^- \rightarrow \underset{\text{Everitt's salt}}{K_2Fe^{II}Fe^{II}(CN)_6} \quad (1)$$

yield a white compound, Everitt's salt. The electrochromic reaction is quite rapid and reversible, with up to 10^7 electrochromic cycles reported for Prussian blue films electrochemically switched under appropriate conditions.[6]

An important factor in both the speed and the long-term reversibility of this electrochemical reaction is undoubtedly the relatively open crystal structure of Prussian blue. This structure features a rigid cubic framework with interstices spacious enough to easily accommodate the compensating ions involved in the reaction (i.e., K^+), thus allowing for a rapid reaction rate and minimal structural disruption.[7] The cubic structure is formed by octahedrally coordinated Fe(III) and Fe(II), which are cyanide-bridged to yield a three-dimensional network of repeating "$-NC-Fe^{II}-CN-Fe^{III}-$" units.

Prussian blue analogues that share this type of cubic framework are well-known. In these compounds other metal ions, typically transition metals, replace either or both types of the iron ions in the structure.[8-10] While many Prussian blue analogues are known, the electrochemical properties of only several have been studied[4,11-16] and the electrochromic properties of still fewer have been well documented.[11,12,15] Given the structural similarities of this family of compounds, Prussian blue analogues seem a fertile area for further electrochemical and spectroelectrochemical investigations.

Recently, the synthesis and electrochemical characterization of films of the Prussian blue analogue vanadium hexacyanoferrate (VHCF) were reported.[17] The films were found to be electro-

* To whom correspondence should be addressed at the Physical Chemistry Department.

(1) Lampert, C. M. *Sol. Energy Mater.* **1984**, *11*, 1.
(2) Goldner, R. B.; Rauh, R. D. *Sol. Energy Mater.* **1984**, *11*, 177.
(3) Carpenter, M. K.; Conell, R. S.; Corrigan, D. A. *Sol. Energy Mater.* **1987**, *16*, 333.
(4) Itaya, K.; Uchida, I.; Neff, V. D. *Acc. Chem. Res.* **1986**, *19*, 162.
(5) Itaya, K.; Shibayama, K.; Akahoshi, H.; Toshima, S. *J. Appl. Phys.* **1982**, *53*, 804.
(6) Itaya, K.; Uchida, I.; Toshima, S. *Denki Kagaku* **1982**, *50*, 436.
(7) Keggin, J. F.; Miles, F. D. *Nature* **1936**, *137*, 577.
(8) van Bever, A. K. *Recl. Trav. Chim. Pays-Bas* **1938**, *57*, 1259.
(9) Brown, D. B.; Shriver, D. F. *Inorg. Chem.* **1969**, *8*, 37.
(10) Ayers, J. B.; Waggoner, W. H. *J. Inorg. Nucl. Chem.* **1971**, *33*, 721.
(11) Rajan, K. P.; Neff, V. D. *J. Phys. Chem.* **1982**, *86*, 4361.
(12) Itaya, K.; Ataka, T.; Toshima, S. *J. Am. Chem. Soc.* **1982**, *104*, 4767.
(13) Bocarsly, A. B.; Sinha, S. *J. Electroanal. Chem. Interfacial Electrochem.* **1982**, *137*, 157. Bocarsly, A. B.; Sinha, S. *J. Electroanal. Chem. Interfacial Electrochem.* **1982**, *140*, 167.
(14) Kulesza, P. J.; Faszynska, M. *J. Electroanal. Chem. Interfacial Electrochem.* **1988**, *252*, 461.
(15) Siperko, L. M.; Kuwana, T. *J. Electrochem. Soc.* **1983**, *130*, 396.
(16) Sinha, S.; Humphrey, B. D.; Bocarsly, A. B. *Inorg. Chem.* **1984**, *23*, 203.
(17) Shaojun, D.; Fengbin, L. *J. Electroanal. Chem. Interfacial Electrochem.* **1986**, *210*, 31.

0020-1669/90/1329-0845$02.50/0

chromic, and the pertinent redox chemistry was reported to involve both the iron and vanadium ions in the compound. In this paper, we characterize VHCF films and their spectroelectrochemistry more fully and present evidence which indicates that the electrochromic reaction involves only the iron ions in the films.

Experimental Section

Sample Preparation. Pt-disk substrates, 1.6 mm in diameter and mounted in Kel-F, were obtained from Bioanalytical Systems, Inc. The electrodes were polished with 0.3-μm alumina powder, soaked in 50% HNO_3, and rinsed with distilled water prior to VHCF deposition.

Glass substrates, coated on one side with a ~440-nm film of conductive fluorine-doped tin oxide (FTO), were obtained from the Watkin-Johnsons Co. (Scotts Valley, CA). Optical transmittance of the coated glass substrate was about 80% throughout the visible region. The FTO film resistance, determined by four-point probe measurements, was ~14 Ω/square. The substrates were 0.3-cm thick and measured 0.9 cm × 5.0 cm, although the actual working area was 0.9 cm × 3.0 cm. Electrical contact to the FTO film was made through a spring clip of 0.1-mm thick nickel foil. The substrates were washed with detergent (Alconox) and rinsed with distilled water prior to VHCF deposition.

Films of VHCF were deposited potentiodynamically from a freshly prepared solution containing 3.6 M H_2SO_4, 0.02 M Na_3VO_4, and 0.02 M $K_3Fe(CN)_6$. Substrates were allowed to equilibrate in the solution for 2 min prior to deposition. The potential of the substrate was swept positive from the open circuit potential, to 1.155 V vs SCE, and then swept continuously between 1.155 and 0.355 V for a predetermined period. Films were deposited on FTO-glass substrates with a scan rate of 100 mV/s for 2 min. A scan rate of 200 mV/s was used to deposit VHCF on the Pt disks.

Films used for XPS analysis were cycled several times between 1.155 and 0.355 V in an electrolyte containing 0.1 M K_2SO_4 and 3.6 M H_2SO_4. Cycling was stopped at either potential limit, and that potential was then maintained for over 1 min to ensure complete oxidation or reduction. The samples were immediately removed for XPS analysis.

Characterization. Metal analyses of bulk VHCF films were accomplished by using inductively coupled plasma with atomic emission spectroscopy (ICP/AES). Measurements were performed on solutions containing dissolved films that were prepared in the following manner: VHCF films were deposited on FTO-glass substrates by potentiodynamic cycling as described above for 2.5 or 3.0 min. Several cyclic voltammograms and coulometric charging data were obtained in an electrolyte of 0.1 M K_2SO_4 and 3.6 M H_2SO_4. Each film was then carefully dissolved in 5 mL of preelectrolyzed 1 M KOH, and the resulting solutions were analyzed by ICP/AES.

X-ray diffraction data were obtained by using a Rigaku rotating copper anode source (18 kW, line focus) coupled with a Siemens D-500 diffractometer set up in horizontal mode. A Bragg–Brentano system geometry was used. Data were collected in the step-scan mode with Siemens software, which also allowed the determination of peak location and intensity. Indexing of the patterns was done by Werner's method,[18] and comparison of the data with reference data from the Joint Committee on Powder Diffraction Standards (JCPDS) was done with software based on that developed by Johnson and Vand.[19]

X-ray diffraction patterns were obtained from both electrodeposited films and from precipitate formed by the slow, spontaneous reaction of the VHCF deposition solution itself. VHCF films deposited on FTO-glass slides were rinsed in dilute electrolyte and dried before mounting in a sample holder. Precipitates were filtered out, washed, and mounted in a zero-background holder by using a clear grease.

Electrochemical and Optical Measurements. Electrodeposition and electrochemical experiments were carried out with a standard three-electrode setup. The potential or current was controlled by a Princeton Applied Research (PAR) Model 273 potentiostat/galvanostat. The reference electrode was either a saturated calomel electrode (SCE) or a Hg/Hg_2SO_4 electrode. All potential values are given versus SCE. A Pt-wire counter electrode was used in all experiments. Cyclic voltammograms were obtained from freshly deposited films in an electrolyte containing 0.1 M K_2SO_4 and 3.6 M H_2SO_4. The films were rinsed with electrolyte prior to voltammetric experiments.

In situ optical absorbance spectra were obtained with a Perkin-Elmer Lambda 9 UV–vis–near-IR (double-beam) spectrophotometer operated at a scan rate of 480 nm/min. The sample chamber was modified to allow insertion of electrode leads. A cuvette containing a piece of FTO glass and filled with electrolyte was placed in the reference beam. The spectroelectrochemical cell was assembled in a plastic cuvette as described previously.[3] The counter electrode was ~15 cm of Pt wire (0.5-mm diameter) twisted together and positioned out of the light beam. The cell contained about 1.5 mL of electrolyte.

XPS Measurements. X-ray photoelectron spectra were obtained with a Surface Science Instruments Model SSX-101 spectrometer using a monochromatic Al Kα X-ray source. Survey spectra were acquired with an X-ray spot size of ~600 μm and an analyzer pass energy of 150 eV (analyzer resolution ~1.5 eV), while high-resolution spectra were acquired by using an X-ray spot size of ~300 μm and an analyzer pass energy of 25 eV (analyzer resolution ~0.5 eV). Under these conditions, the full width at half-maximum values (fwhm) for the Au $4f_{7/2}$ transitions used for calibration were 1.4 and 0.7 eV, respectively. Specimens were flooded with ~3-eV electrons during data acquisition to minimize charging effects. Peak energies were referenced to a common scale by setting that for C 1s = 284.8 eV.

Peak position results were compared with published data[20,21] or with data collected from appropriate standards such as $K_4Fe(CN)_6 \cdot 3H_2O$ and $K_3Fe(CN)_6$ to determine the chemical states of the metal atoms. Elemental ratios were calculated after first correcting the raw areas under the photoelectron transitions with Scofield photoionization cross-section[22] and inelastic electron mean free path[23] data.

Results and Discussion

Film Deposition. Films of VHCF were deposited potentiodynamically from 3.6 M H_2SO_4 containing 0.02 M Na_3VO_4 and 0.02 M $K_3Fe(CN)_6$ by using the method of Shaojun and Fengbin.[17] To better understand the deposition process, solutions containing only one of the corresponding reducible ions, either VO_2^+ or ferricyanide ion ($Fe(CN)_6^{3-}$), were examined with cyclic voltammetry. Platinum-disk electrodes were used to obtain the voltammograms shown in Figure 1. From the top panel in Figure 1 it can be seen that the vanadium ion was reduced at potentials positive of $Fe(CN)_6^{3-}$ reduction, as expected from their standard reduction potentials, 0.76 and 0.45 vs SCE, respectively.[24] The differences in peak shape and current density of the two cyclic voltammograms suggest that the reduction of VO_2^+ at platinum is not as reversible as the facile $Fe(CN)_6^{3-}/Fe(CN)_6^{4-}$ couple.

The lower panel of Figure 1 shows current–voltage curves obtained during film deposition. The potential of the platinum disk in the deposition solution was repeatedly swept between 0.355 and 1.155 V vs SCE at 200 mV/s. On the initial sweep, the potential was ramped from the rest potential of the solution, ~1.04 V vs SCE, toward more positive potentials. The absence of current on this portion of the scan reflects the lack of oxidizable material on the electrode or in the solution. On the subsequent sweep in the negative direction, the onset of cathodic current occurred at about 0.88 V. Comparison with the traces in the top panel strongly suggests that this onset was due to the reduction of the vanadium(V) species. The subsequent increases in both anodic and cathodic peak currents seen on successive cycles are consistent with the buildup of a redox-active film on the platinum electrode. The anodic peaks centered at about 0.80 and 0.92 V vs SCE and the corresponding cathodic peaks centered at 0.78 and 0.91 V, respectively, are essentially identical with those reported previously for VHCF.[17]

From Figure 1 it appears that the electrodeposition of VHCF involves the reduction of the VO_2^+ ion in solution. This reduced species then reacts rapidly with ferricyanide ion to form an insoluble complex that precipitates on the electrode surface. While the reduction of the ferricyanide ion in solution probably also occurs when the electrode is swept to more negative potentials, this reduction does not appear to be crucial to film formation, since VHCF films were also successfully deposited by potential cycling

(18) Werner, P. E. *J. Appl. Crystallogr.* **1976**, *9*, 216.
(19) Johnson, G. G.; Vand, V. *Ind. Eng. Chem.* **1967**, *59*(8), 19.
(20) Wagner, C. D. *Practical Surface Analysis by Auger and X-ray Photoelectron Spectroscopy*; Briggs, D., Seah, M. P., Eds.; John Wiley and Sons: New York, 1983; Appendix 4, p 494.
(21) Wagner, C. D.; Riggs, W. M.; Davis, L. E.; Moulder, J. F.; Muilenberg, G. E. *Handbook of X-ray Photoelectron Spectroscopy*; Physical Electronics Industries: Eden Prairie, MN, 1979; pp 76, 77.
(22) Scofield, J. H. *J. Electron Spectrosc.* **1976**, *8*, 129.
(23) Seah, M. P.; Dench, W. A. *Surf. Interface Anal.* **1979**, *1*, 2.
(24) *Handbook of Chemistry and Physics*, 55th ed.; CRC Press: Cleveland, OH, 1974; pp D-120, 122.
(25) Ibers, J. A.; Davidson, N. *J. Am. Chem. Soc.* **1951**, *73*, 476.

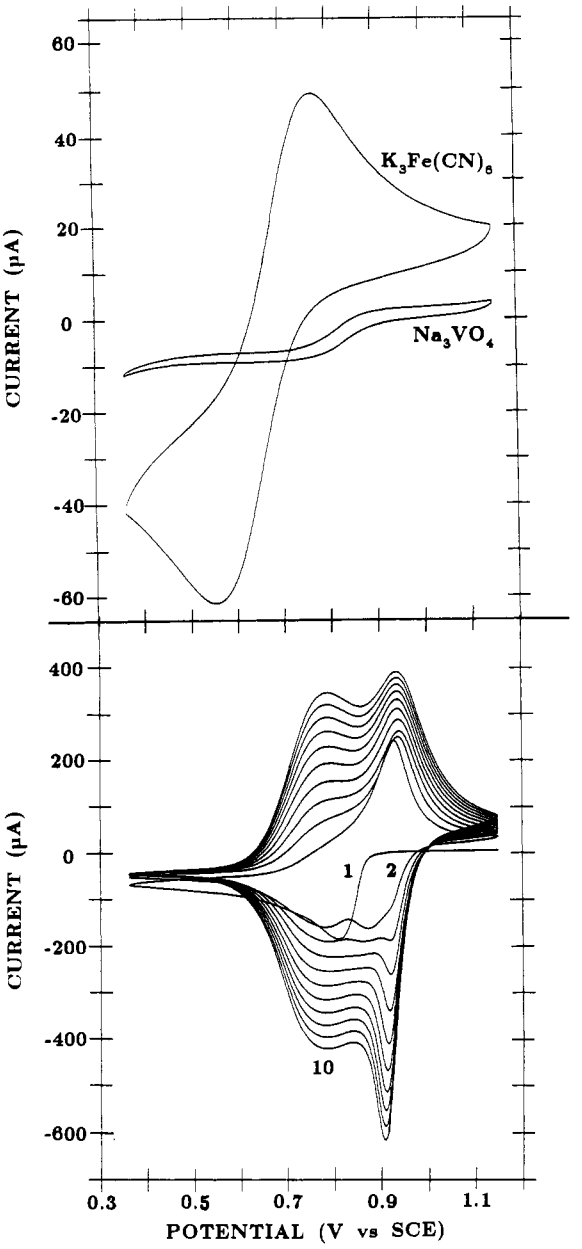

Figure 1. Top panel: Cyclic voltammorgrams of single-component solutions, 0.02 M Na_3VO_4 and 0.02 M $K_3Fe(CN)_6$. Bottom panel: Cyclic voltammetry of VHCF deposition solution containing both 0.02 M Na_3VO_4 and 0.02 M $K_3Fe(CN)_6$. The first 10 scans are shown (scans 1, 2, and 10 are labeled). A Pt-disk working electrode and a scan rate of 200 mV/s were used for both panels. Positive currents are anodic; negative currents are cathodic.

between 1.155 and 0.8 V—positive of the potential required for ferricyanide reduction at platinum.

Although the electrodeposition of Prussian blue from an analogous solution containing $K_3Fe(CN)_6$ and $Fe_2(SO_4)_3$ is known to involve the complex $Fe^{III}[Fe^{III}(CN)_6]$, we found no evidence from UV–vis spectra to suggest the formation of a similar V-$[Fe^{III}(CN)_6]$-type complex in the VHCF deposition solution. The spectrum of the deposition solution appeared to be a simple summation of spectra from the single-component solutions.

Composition and Structure. X-ray diffraction data from electrodeposited films support the description of VHCF as a Prussian blue analogue. Specifically, VHCF retains a cubic framework similar to that of Prussian blue, presumably with vanadium ions substituted for the ferric ions in the N-bonded sites. The three diffraction peaks obtained from VHCF films correlate well with the 200, 220, and 400 peaks reported for Prussian blue.[19] In addition, the powder pattern in Figure 2, from a VHCF precipitate, exhibits the same three peaks, as well as a number of

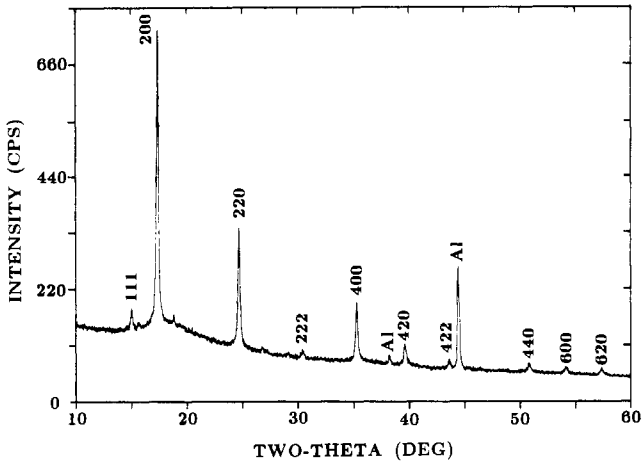

Figure 2. X-ray powder diffraction data from VHCF precipitate. Peaks are marked with *hkl* assignments. Peaks due to the aluminum sample holder are marked "Al".

Table I. X-ray Diffraction Data[a]

Prussian blue		VHCF		
d, Å	*I*(rel)	*d*, Å	*I*(rel)	*hkl*
		5.87	6.2	111
5.10	100	5.08	100.0	200
3.60	32	3.59	39.7	220
		2.93	4.7	222
2.55	48	2.53	19.8	400
2.28	32	2.27	8.5	420
2.07	3	2.07	3.8	422
1.80	14	1.79	3.4	440
1.70	13	1.70	3.7	600
1.61	14	1.60	2.0	620

[a] Peak intensities, *I*, given as relative values. Prussian blue data from JCPDS, PDF No. 1-239.

smaller peaks that correlate closely with those obtained from Prussian blue. The *d* spacings and intensities of the diffraction peaks of both the VHCF precipitate and Prussian blue are listed in Table I for comparison. While the 111 and 222 peaks of VHCF are not matched by peaks in the Prussian blue powder data cited, we note that more recent X-ray data, from thin-film and single-crystal Prussian blue, have shown the presence of these peaks.[26]

While we refer to VHCF as a Prussian blue analogue, we note that there are actually two forms of Prussian blue known, the so-called "soluble" and "insoluble" forms (these terms refer to peptization rather than solubility). The soluble form, $KFe[Fe(CN)_6]$, has a face-centered cubic crystal structure,[7] with potassium ions occupying interstices in the cubic framework, while insoluble Prussian blue, $Fe_4[Fe(CN)_6]_3 \cdot xH_2O$, shares the same basic cubic structure, except that one-fourth of the ferrocyanide ions are absent.[26,27] Shaojun and Fengbin[17] suggested the composition of the reduced VHCF films to be $KV[Fe(CN)_6]$, in close analogy to the composition of soluble Prussian blue. However, ICP/AES analysis of the metal atom content in our VHCF films gives a vanadium to iron ratio of 1.50 ± 0.03, instead of the value of unity expected for a direct analogue of soluble Prussian blue. The measured value is also larger than the 1.33 ratio predicted for an insoluble Prussian blue analogue but is consistent with the formula $K_2(VO)_3[Fe(CN)_6]_2 \cdot 11.5H_2O$ reported by Ayers and Waggoner[10] for a precipitate formed by the reaction of vanadyl ions with ferrocyanide.

The apparent discrepancy between a V/Fe ratio of 1.5 and the retention of a regularly substituted Prussian blue structure can

(26) Buser, H. J.; Schwargenbach, D.; Petter, W.; Ludi, A. *Inorg. Chem.* **1977**, *16*, 2704. Ikeshoji, T.; Iwasaki, T. *Inorg. Chem.* **1988**, *27*, 1123.
(27) Ludi, A.; Gudel, H. U. *Structure and Bonding*; Dunitz, J. D., Hemmerich, P., Ibers, J. A., Jorgenson, C. K., Neilands, J. B., Nyholm, R. S., Reinen, D., Williams, R. J. P., Eds.; Springer-Verlag: New York, 1973; Vol. 14, pp 1–21.

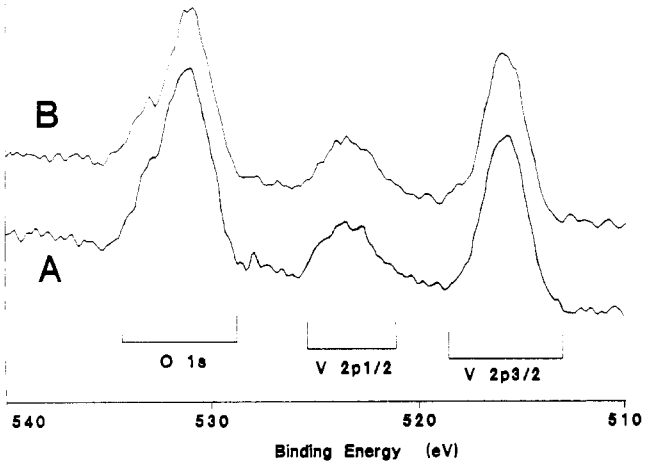

Figure 3. X-ray photoelectron spectra of the V $2p_{3/2}$, V $2p_{1/2}$, and O 1s transitions from reduced (A) and oxidized (B) VHCF films.

be reconciled by the presence of interstitial vanadium ions, since such ions would increase the relative vanadium content without disrupting the cubic framework. Similar interstitial ferric ions are often present in freshly precipitated samples of Prussian blue.[28] Vanadium interstitials would also account for the 1.1–1.5 range of surface V/Fe ratios that were found by using XPS; varying degrees of replacement of the interstitial vanadium ions near the surface by potassium ions from the electrolyte solution would yield surface V/Fe ratios less than 1.5. Complete substitution of the interstitials would yield a ratio of 1.

The XPS spectra in Figure 3 indicate the majority of vanadium in the films is present as V(IV) on the basis of the peak position of the V $2p_{3/2}$ transition (BE = 516.1 eV). This assignment is consistent with binding energies reported for other V(IV) compounds (BE = 515.8–516.2 eV).[21] Binding energy peaks from compounds containing V(III) or V(V) are typically displaced at least 0.5 eV from the binding energy peak of VHCF.[21] In conjunction with the infrared identification of V–O bonds in VHCF,[17] it is clear that at least some of the vanadium atoms are present as vanadyl ions, VO^{2+}, in VHCF. If these ions are bonded into the VHCF lattice, then some disruption of the cyanide-bridged lattice would be required to accommodate them. Whereas a simple substitution of V into a Prussian blue lattice would yield V atoms octahedrally coordinated by the N atoms in bridging CN ligands, the incorporation of VO^{2+} might yield nominally octahedral vanadium atoms coordinated by a terminal oxygen and only five bridging cyanide ligands. Such disruption would result in multiple iron sites in the compound: iron ions bonded exclusively to bridging cyanides, iron ions coordinated to one or more terminal cyanides, and perhaps iron ions bonded to one or more non-cyanide ligands, such as H_2O. As discussed below, the presence of two or more iron sites is consistent with the electrochemistry found for VHCF.

Electrochemistry. Vanadium hexacyanoferrate films on conductive substrates can be electrochemically oxidized and reduced in acidic electrolytes containing potassium ion, as indicated by the cyclic voltammograms in Figure 4. The traces shown are from a VHCF film deposited on FTO-coated glass and are quite similar to those reported previously for VHCF films on Pt substrates,[17] although the scan rate is much slower. The major features are two anodic and two cathodic peaks. A third peak was reported for VHCF on Pt in more acidic electrolytes, but we were unable to duplicate this result on either FTO glass or Pt substrates. Figure 4 shows that the amount of charge involved in the redox reactions decreased significantly after 10 potentiodynamic cycles, indicative of some film dissolution, in contrast to the good stability reported for VHCF films on Pt.[17] The apparent rate of dissolution of our films did, however, slow significantly with successive scans.

(28) Bonnette, A. K., Jr.; Gandy, S. E. *J. Chem. Educ.* **1981**, *58*, 355.

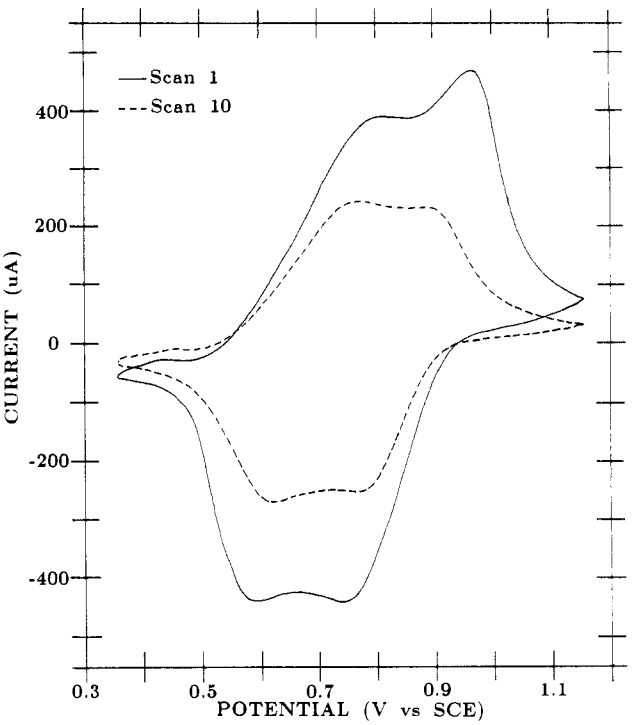

Figure 4. Cyclic voltammograms of VHCF on FTO-coated glass. The electrolyte was 0.1 M K_2SO_4 and 3.6 M H_2SO_4, and the scan rate was 10 mV/s.

Shaojun and Fengbin[17] attributed the three redox waves of their VHCF films to the following reactions:

$$K^+V^{3+}Fe^{II}(CN)_6 + H_2O + K^+ \rightarrow K^+_2VO^{2+}Fe^{II}(CN)_6 + 2H^+ + e^- \quad (2)$$

$$K^+_2VO^{2+}Fe^{II}(CN)_6 + H_2O \rightarrow K^+_2(VO_2H)^+Fe^{III}(CN)_6 + H^+ + e^- \quad (3)$$

$$K^+_2(VO_2H)^+Fe^{III}(CN)_6 + 2H_2O + K^+ \rightarrow K^+_2(VO_2)^+Fe^{III}(CN)_6 + H^+ + e^- \quad (4)$$

Of note is that both metal centers are involved in this reaction scheme, with vanadium ions oxidized in reactions 2 and 4 and ferrocyanide ion oxidized in reaction 3.

To determine the validity of this scheme, we examined a number of electrochemically oxidized (1.155 V) and reduced (0.355 V) VHCF films on both Pt and FTO-glass substrates with high-resolution XPS. Figure 3 shows representative spectra of the V $2p_{3/2}$ and $2p_{1/2}$ transitions from both a fully reduced and a fully oxidized film. Surprisingly, the spectra are essentially identical, indicating that the oxidation state of the vanadium ions in VHCF is the same in both oxidized and reduced films. Thus, the vanadium ions are apparently not electrochemically active in VHCF films.

An alternate explanation for the lack of change in our XPS results might be a rapid air reoxidation of electrochemically reduced vanadium at the film surface. However, we obtained similar results in later experiments that were carried out under nitrogen and with minimal air exposure of the sample during transfer to the vacuum chamber of the XPS instrument. In addition, visual evidence did not suggest that rapid air oxidation of VHCF was occurring—the reduced films retained their yellow color upon standing for long periods in air. (Oxidized films are green.)

The distinct changes seen in the XPS spectra of the Fe $2p_{3/2}$ and $2p_{1/2}$ transitions from oxidized and reduced VHCF films (Figure 5) do indicate that iron ions are directly involved in the redox reaction(s) of VHCF. The spectrum of the reduced film, shown in curve A, exhibits a single, sharp Fe $2p_{3/2}$ transition with a binding energy of 708.2 eV, which we attribute to ferrocyanide ion. Curve B, from an oxidized film, exhibits an additional

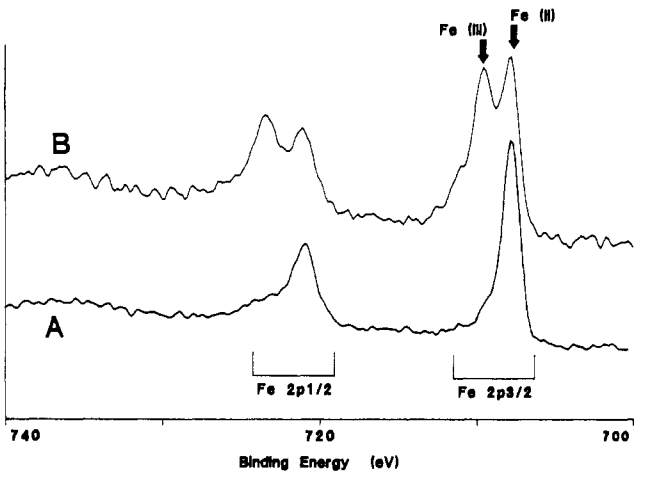

Figure 5. X-ray photoelectron spectra of the Fe $2p_{3/2}$ and Fe $2p_{1/2}$ transitions from reduced (A) and oxidized (B) VHCF films.

Table II. Charge Required to Oxidize VHCF Films

V charge,[a] mC	Fe charge,[a] mC	predicted charge,[b] mC	actual charge,[c] mC
90	61	241	65
111	72	294	60
86	57	229	60

[a] Amount of charge required for a one-electron oxidation of all V or Fe ions in a film. All calculated charges based on metal contents obtained from ICP analyses. [b] Total charge predicted by reactions 2–4 to completely oxidize the film. [c] The total charge measured during oxidiation of the film.

transition that was identified as arising from ferricyanide ion, as expected from the electrochemical oxidation of ferrocyanide. Similar results have been reported for another Prussian blue analogue, copper hexacyanoferrate.[15]

Coulometric experiments were performed to determine the amount of charge injected into the films during oxidation. Several films on FTO glass were galvanostatically oxidized at 500 μA to the completion of the reaction and then dissolved in base and analyzed by ICP to determine the amounts of vanadium and iron present in each film. The results of these experiments, together with predicted charge values, are given in Table II. The total charge predicted for the oxidation of the films, on the basis of the reaction scheme of eq 2–4, can be seen to be about four times greater than the amount of charge actually required. While the actual amount of charge used was insufficient to oxidize both the ferrocyanide and vanadium ions in the films, the measured charge closely approximates the amount of charge that would be required to oxidize only the ferrocyanide ions. This is consistent with the XPS results which show that only the iron atoms are involved in the redox reaction(s) of VHCF.

While both the XPS and coulometric data provide strong evidence that vanadium ions are not involved in the redox chemistry of the films, the presence of at least two oxidation and reduction peaks in the cyclic voltammograms does indicate that there is more than one electrochemical process occurring in VHCF. Such multiple redox peaks might be explained by the presence of multiple ferrous sites. As noted above, disruption of the simple cyanide-bridged lattice by the incorporation of vanadyl ions would result in several types of ferrous sites, which might be expected to have slightly different oxidation potentials. A somewhat similar situation has been reported by Lundgren and Murray[29] in which two types of ferric sites in films of Prussian blue gave rise to complex reduction behavior.

Interestingly, cyclic voltammograms reported for the oxidation of Prussian blue appear quite similar to our voltammograms of VHCF in that they exhibit two oxidation peaks at potentials similar to those of VHCF.[12,30,31] This similarity of voltammograms is not suprising if, as our results indicate, the redox chemistry of VHCF involves the oxidation of (nominally) ferrocyanide sites, since the oxidation of Prussian blue involves the oxidation of similar ferrocyanide sites. While the presence of dual oxidation peaks for Prussian blue has not been well explained, the similarities in the electrochemistries of VHCF and Prussian blue further support the notion that only the ferrocyanide moiety is electrochemically active in VHCF.

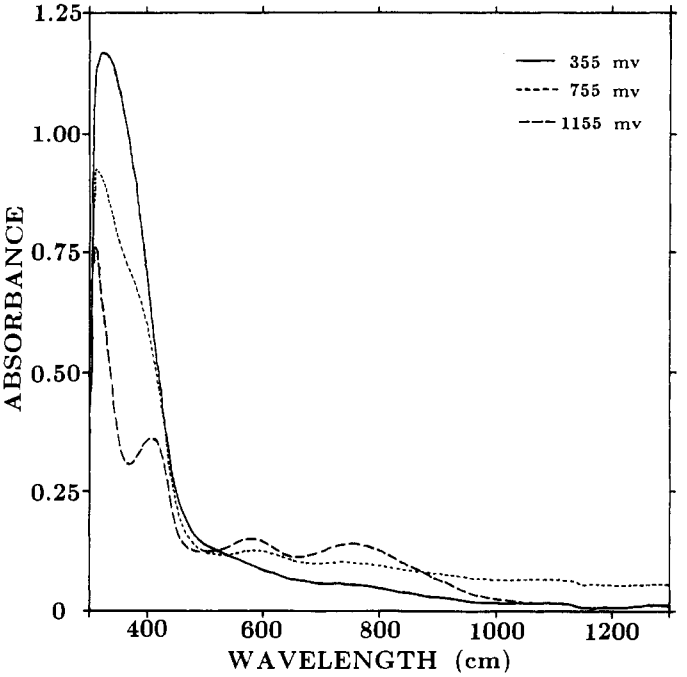

Figure 6. Optical absorbance spectra of a VHCF film on FTO-coated glass in electrolyte containing 0.1 M K_2SO_4 and 3.6 M H_2SO_4. The film was maintained at the potentials noted.

Optical Measurements. Electrochromism in VHCF films is seen visually as a color change from yellow to green when a reduced film is oxidized. To better quantify this change, absorbance spectra of VHCF films on FTO-coated glass were taken in situ with the films held at various potentials. Representative spectra of one film, held at three different potentials, are shown in Figure 6. From the figure it is clear that although the films are electrochromic in the visible region of the spectrum, the major electrochromic modulation actually occurs in the ultraviolet (UV) region of the spectrum. In addition, the absence of a strong absorption band at 690 nm (at any potential) indicates that Prussian blue is not a significant component of the VHCF films.

The dominant feature in the spectrum of the reduced film (355 mV) is seen in the UV region as an absorption band around 370 nm, although the full shape of the band is obscured at wavelengths smaller than 360 nm by instrumental complications caused by the strong absorption of the FTO-glass substrate. Upon oxidation of the film at 1115 mV, the 370-nm band gives way to another strong absorption band with an apparent maximum below 350 nm and a smaller peak at 410 nm. The large intensities of the strongest UV bands of both the oxidized and reduced films suggest that these bands arise from a charge-transfer transition.

In the visible region, the spectrum of the reduced film shows a weak, broad absorbance tail trailing from the UV band. This tail is responsible for the yellow color. The green color of the oxidized film is due to two small peaks centered at 580 and 760 nm. Of particular interest in the spectrum of oxidized VHCF are peaks at 410 and 760 nm, which are similar to peaks seen in the spectrum of oxidized Prussian blue (Berlin green) at 420 and 780 nm.[12] Given the chemical similarity of the two materials, we suggest that both sets of peaks involve electronic transitions

(29) Lundgren, C. A.; Murray, R. W. *Inorg. Chem.* **1988**, *27*, 933.

(30) Goncalves, R. M. C.; Kellawi, H.; Rosseinsky, D. R. *J. Chem. Soc., Dalton Trans.* **1983**, 991.

(31) Ellis, D.; Eckhoff, M.; Neff, V. D. *J. Phys. Chem.* **1981**, *85*, 1225.

associated with ferricyanide sites.

The absorbance spectrum of the partially oxidized film (0.755 V) is intermediate between those of the fully oxidized and reduced film, except for an increase in the near-infrared portion of the spectrum (at wavelengths greater than 900 nm). The absorption increase in this region is reproducible, but its origin is uncertain. Since the voltammetric data suggest that two oxidation processes occur in VHCF, this absorption band may arise from VHCF that has undergone only the first oxidation step. The lack of an isosbestic point in Figure 6 is consistent with the presence of at least two oxidation processes for VHCF.

Acknowledgment. We are grateful to Michael Balogh and Audrey Dow for ICP measurements and XPS data collection, respectively. We also thank G. A. Nazri for helpful discussions and the Watkins-Johnson Co. (Scotts Valley, CA) for their donation of FTO-coated glass substrates.

Registry No. VHCF, 89184-12-3; TO, 18282-10-5; F_2, 7782-41-4; Pt, 7440-06-4; Na_3VO_4, 13721-39-6; $K_3Fe(CN)_6$, 13746-66-2; K_2SO_4, 7778-80-5; H_2SO_4, 7664-93-9.

Contribution from the Department of Chemistry, North Dakota State University, Fargo, North Dakota 58105

Relationship of the Ruby Spectrum to the Geometry of the Chromium(III) Environment

Kyu-Wang Lee and Patrick E. Hoggard*

Received July 12, 1988

The electronic spectrum of ruby has been fit by using the angular overlap model (AOM) to express the total ligand field potential at the Cr^{3+} site from the nearest 813 oxide ions and 542 aluminum ions. The optimized AOM parameter values were $e_{\sigma O}$ = 8867 cm^{-1} and $e_{\pi O}$ = 853 cm^{-1} for the oxide ions nearest to the chromium and $e_{\sigma Al}$ = −9275 cm^{-1} for the nearest Al^{3+}, with $e_{\pi Al}$ fixed at zero. The oxide ion AOM parameters were constrained to decline with the distance from Cr^{3+} as R^{-3}, while $e_{\sigma Al}$ was reduced as R^{-5}. The relatively small value of $e_{\pi O}$ results from a distribution of the oxide ion electron donor properties among a distorted tetrahedron of aluminum ions.

Introduction

The electronic structure of ruby (Cr^{3+} doped in α-alumina) is of both historical and practical interest, and a considerable effort has been invested in the measurement of the transition energies to the d–d excited states and in the use of ligand field theory to calculate these transition energies, beginning with the pioneering work of Sugano et al.[1-3] on the effects of a trigonally distorted crystal field. The electronic spectrum of ruby is more completely and more accurately known than that of any other Cr(III) system,[4-13] with the exception of the free ion, and thus constitutes a particularly important challenge to ligand field theory.

All previous treatments have been based on the actual C_3 or approximate C_{3v} symmetry of the Cr^{3+} ion site, and the one-electron ligand field potential matrix has been developed from a generalized trigonal potential, which may be expressed as the sum of an octahedral potential and additional terms allowed in the trigonal symmetry.[14,15] The ligand potential matrix, $\langle d_i|V|d_j\rangle$, has a minimum of four unrelated nonzero elements, which may be expressed by using C_3 (O_h) labels for the d orbitals as $\langle e(t_2)|V|e(t_2)\rangle$, $\langle e(e)|V|e(e)\rangle$, $\langle e(t_2)|V|e(e)\rangle$, and $\langle a_1(t_2)|V|a_1(t_2)\rangle$. Since only energy differences are observed, one of these is arbitrary, and the trigonal field can be evaluated with three parameters. Generally these are chosen as an octahedral parameter Δ, equal to the energy difference between $e(e_g)$ and the center of gravity of the t_{2g} orbitals, and two trigonal perturbation terms, one representing the (diagonal) splitting within the t_{2g} orbitals, and the other, sometimes neglected,[1] the off-diagonal element $\langle e(t_2)|V|e(e)\rangle$.

In their attempt to model the ruby spectrum, Sugano and Peter started with nine parameters: the three ligand field parameters, two spherical interelectronic repulsion parameters (the Racah parameters B and C), two spin–orbit coupling parameters (one between t_{2g} orbitals and one between a t_{2g} and an e_g orbital), and two orbital reduction parameters, defined like the spin–orbit coupling parameters.[3] This set of parameters was effectively reduced by two by the assumption that the pairs of trigonal field, spin–orbit coupling, and orbital reduction parameters stand in the same relationship. It was further reduced to a total of six adjustable parameters by fixing the value of C at $4B$. The secular determinants were derived only from the t_{2g} and $t_{2g}^2e_g$ configurations, and no optimization procedure was used to find the global minimum. The orbital reduction factors k and k' were used in the magnetic field dependent portion of the Hamiltonian.[16] Normally these parameters would affect only the g values determined from Zeeman splittings, but by being subjected to a relationship with the spin–orbit coupling and trigonal field parameters, the value of k also affected the zero-field transition energies. The calculations were applied only to states from the t_{2g}^3 configuration, including the zero-field splitting (ZFS) of the $^4A_{2g}$ ground state, and their results are shown in Table I.

Macfarlane in 1963 improved on this calculation by including all configurations in setting up the secular determinant.[17] Although final energy eigenvalues were determined by diagonalizing the matrices within each C_{3v}* double-group representation, parameter refinement had to be carried out by means of perturbation expressions. The six-parameter set used by Macfarlane consisted of the three ligand field parameters, the Racah parameters B and C, and a single spherical spin–orbit coupling parameter. The results, shown in Table I, reproduce the sharp-line splittings rather well, although the term energies themselves are not nearly as well fit.

(1) Sugano, S.; Tanabe, Y. *J. Phys. Soc. Jpn.* **1958**, *13*, 880.
(2) Sugano, S. *Suppl. Prog. Theor. Phys.* **1960**, *No. 14*, 66.
(3) Sugano, S.; Peter M. *Phys. Rev.* **1961**, *122*, 381.
(4) Deutschbein, O. *Ann. Phys.* **1932**, *14*, 712.
(5) Deutschbein, O. *Ann. Phys.* **1932**, *14*, 729.
(6) Deutschbein, O. *Ann. Phys.* **1932**, *20*, 828.
(7) Sugano, S.; Tsujikawa, I. *J. Phys. Soc. Jpn.* **1958**, *13*, 899.
(8) Low, W. *J. Chem. Phys.* **1960**, *33*, 1162.
(9) McClure, D. S. *J. Chem. Phys.* **1962**, *36*, 2757.
(10) Margerie, J. *C. R. Hebd. Seances Acad. Sci.* **1962**, *255*, 1598.
(11) Nelson, D. F.; Sturge, M. D. *Phys. Rev.* **1965**, *137*, A1117.
(12) Powell, R. C.; DiBartolo, B.; Birang, B.; Naiman, C. S. *Phys. Rev.* **1967**, *155*, 296.
(13) Fairbank, W. M., Jr.; Klauminzer, G. K.; Schawlow, A. L. *Phys. Rev. B* **1975**, *11*, 60.
(14) Ballhausen, C. J. *Introduction to Ligand Field Theory*; McGraw-Hill: New York, 1962; p 103.
(15) Pryce, M. H. L.; Runciman, W. A. *Discuss. Faraday Soc.* **1958**, *26*, 34.
(16) Stevens, K. W. H. *Proc. R. Soc. London* **1954**, *A219*, 542.
(17) Macfarlane, R. M. *J. Chem. Phys.* **1963**, *39*, 3118.

0020-1669/90/1329-0850$02.50/0